Pergamon

Int. J. Heat Mass Transfer. Vol. 37, No. 5, pp. 783–801, 1994

0017–9310/94 $6.00+0.00

Experimental and numerical analyses of the natural convection of water through its density maximum in a rectangular enclosure

M. W. McDONOUGH and A. FAGHRI

Department of Mechanical and Materials Engineering, Wright State University, Dayton, OH 45435, U.S.A.

(*Received* 26 *April* 1993 *and in final form* 13 *August* 1993)

Abstract—An experimental and numerical investigation is presented concerning the transient and steady-state natural convection of water through its density maximum in a rectangular enclosure with the vertical end walls held at different temperatures. The water in the enclosure is initially at a uniform temperature above the density maximum at 3.98°C, and then the temperature of the cold wall is suddenly reduced to and maintained at 0°C. Experimental flow patterns are presented for 5 and 8°C initial and hot wall temperatures. A pH indicator technique is used to visualize the convective flow patterns in the enclosure. Numerical solutions of the convective flow patterns are presented for transient and steady-state natural convection, and are shown to be in good agreement with experimental flow patterns. The effect of the density inversion on the transient convective flow patterns was dominant at a 5°C initial and hot wall temperature. Steady-state results for an 8°C initial and hot wall temperature show an asymmetric convective flow pattern with the dominant flow cell being above the density inversion.

INTRODUCTION

NATURAL convection in enclosures has been the subject of experimental and numerical research over the past two decades due to its importance in applications such as materials processing, solar energy systems, and thermal energy storage systems. A review of natural convection in enclosures was given by Ostrach [1]. The majority of these studies are concerned with fluids whose density–temperature relationship can be approximated by the Boussinesq approximation in which the density is assumed to be a linear function of temperature. However, water has a density maximum at 3.98°C, and thus the coefficient of thermal expansion changes sign through this maximum. For water cooled through its density maximum, the linear approximation, $\rho \simeq \rho_0[1-\beta(T-T_0)]$, is not valid. Previous experimental and numerical investigations of the natural convection of water have included the density inversion for a variety of geometries and boundary conditions.

Watson [2] numerically studied the effect of the density inversion of water on natural convection in a rectangular enclosure. Watson examined the steady two-dimensional natural convection in a square enclosure with isothermal vertical walls and adiabatic horizontal walls. Bicellular-flow patterns for hot wall temperatures between 6 and 10°C, and for Rayleigh numbers below 2×10^4 were found.

The transient natural convection of water in a horizontal cylinder with a constant cooling rate through 4°C and for a Rayleigh number range of 10^5 to 2×10^6 was examined by Cheng and Takeuchi [3]. The transient nature of the flow pattern in the horizontal cylinder was shown to begin as a single cell flow above the density inversion, then a bicellular flow pattern existed when the temperature gradient in the cylinder passed through the density inversion temperature, and finally a single cell flow pattern existed when the temperature was below the density inversion.

Vasseur and Robillard [4] numerically investigated the transient natural convection of water in a rectangular enclosure with different aspect ratios and initial water temperatures varying from 4 to 21°C. The vertical walls of the enclosure were isothermal at 0°C and the horizontal walls were adiabatic. Their results showed three stages in the flow pattern. First, a single cell flow existed when the temperature was above the density inversion. Second, a bicellular flow with counter-rotating cells was present when the temperature encompassed the density inversion. Finally, a single cell flow returned when the temperature was below the density inversion. Only results for a Rayleigh number range of 2.9×10^3 to 8.0×10^4 were presented.

The steady natural convection heat transfer of water within a horizontal cylindrical annulus with density inversion effects was numerically studied by Vasseur *et al.* [5]. With each cylinder wall at a different isothermal temperature above and below the density inversion, the results show that the steady-state flow pattern in the annulus was bicellular with a clockwise flow below the density inversion and a counter-clockwise flow above the density inversion. Results were only presented for Rayleigh numbers in the range of 2×10^3 to 7.6×10^4.

Inaba and Fukuda [6] experimentally studied the steady natural convection of water in an inclined rec-

NOMENCLATURE

g	gravitational acceleration, 9.8 m s^{-2}
H	height of enclosure [m]
k	thermal conductivity [W m^{-1} K^{-1}]
p	pressure [Pa]
P	dimensionless pressure, $H^2(p+\rho_0 gy)/(\rho_0\alpha^2)$
Ra	Rayleigh number
Ra^*	modified Rayleigh number
T	temperature [K]
T^*	dimensionless temperature, $(T-T_f)/(T_h-T_c)$
T_i	initial temperature [K]
T_i^*	initial dimensionless temperature, $(T_i-T_f)/(T_h-T_c)$
T_c	cold wall temperature [K]
T_c^*	dimensionless cold wall temperature, $(T_c-T_f)/(T_h-T_c)$
T_h	hot wall temperature [K]
T_h^*	dimensionless hot wall temperature, $(T_h-T_f)/(T_h-T_c)$
t	time [s]
u	x-direction velocity [m s^{-1}]
v	y-direction velocity [m s^{-1}]
U, V	dimensionless velocities, uH/α, vH/α
$\vec{V}$	resultant velocity [m s^{-1}]
x, y	coordinate directions
X, Y	dimensionless coordinate directions, x/H, y/H.

Greek symbols

α	thermal diffusivity [m^2 s^{-1}]
β	coefficient of thermal expansion [K^{-1}]; coefficient equation (13)
μ	dynamic viscosity [kg m^{-1} s^{-1}]
ρ	density [kg m^{-3}]
ρ_0	reference density [kg m^{-3}]
τ	dimensionless time, $\alpha_1 t/H^3$.

tangular cavity with opposing walls at different temperatures. The cold wall was maintained at 0°C and the hot wall was varied from 4 to 20°C and the test cell was inclined for 0 to 180° at 30° increments for each experiment. It was shown that both the density inversion and the inclination angle influenced the convective flow pattern present in the cavity.

The steady natural convection of water in a narrow vertical enclosure for a Rayleigh number range of 10^8–10^{11} was presented by Lankford and Bejan [7]. When the hot and cold wall temperatures encompassed the density inversion temperature, the natural convective flow pattern was shown to be characterized by two counter-rotating cells.

Braga and Viskanta [8] experimentally and numerically investigated the transient natural convection of water in a rectangular cavity with a free surface. Comparisons were made between experimental results and numerical predictions of the flow patterns and temperature distributions for a cold wall temperature of 0°C and hot wall temperatures of 8, 12, 16, and 20°C. It was shown that predicted flow patterns were in good agreement with experimental results. Only the first 30 min of the transient numerical solutions were presented due to the large amount of computer time required to obtain a converged solution.

The motivation for the present investigation was the need to understand the transient nature of the convective flow under the influence of the density inversion during the solidification of water in a rectangular cavity [9]. Experiments were conducted in a rectangular enclosure with one vertical wall suddenly reduced to and maintained at 0°C, and the other vertical wall maintained at 5 and 8°C. For each experiment the water was initially stagnant and at the hot wall temperature. The convective flow patterns were visualized by a pH indicator technique. A mathematical model was developed which included the effects of the density inversion. The conservation equations were solved numerically using a control-volume based finite-difference method. The present investigation differs from previous ones in that both the transient and steady-state natural convection of water relatively near its density maximum (5 and 8°C) has been investigated in a rectangular enclosure at a high Rayleigh number ($Ra > 10^7$). Quantitative and qualitative experimental results are also presented for both the transient and steady-state cooling process.

EXPERIMENTAL METHODOLOGY

The experimental apparatus has three main components: the test cell, recirculating chillers and coolant flow system, and the flow visualization instrumentation. The test cell had a rectangular cross-section with opposing vertical walls held at constant temperatures, and the top, bottom and sides were insulated. Figure 1 shows the details of the test cell where the dimensions are $160 \times 120 \times 120$ mm ($L \times W \times H$). A multipass flat plate heat exchanger was used to provide a uniform isothermal condition on the vertical wall which was held at 0°C for each experiment. The multipass function, in which adjacent tubes have opposing coolant flows, was achieved by a manifold constructed of cast acrylic and attached to the copper tubes with plastic tubing. This arrangement ensured the most uniform temperature for the copper plate.

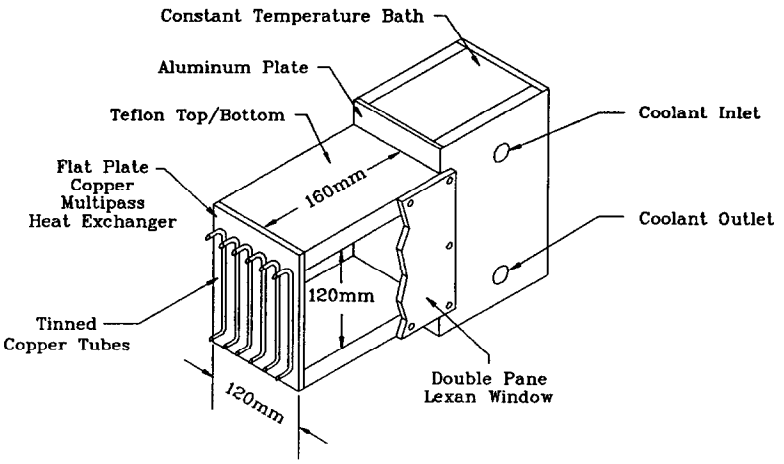

FIG. 1. Rectangular test cell with constant temperature bath and multipass heat exchanger.

Opposite the heat exchanger is a constant temperature bath as shown in Fig. 1. An aluminum plate 1.59 mm thick was used as the side of the constant temperature bath which faced the interior of the test cell. Two coolant inlets and two outlets were placed on the opposing sides of the bath, with the inlets at the top and the outlets at the bottom of the bath (Fig. 1). This arrangement of coolant flow was designed so that the coolant in the bath would be well mixed, which maintained a constant temperature at the aluminum plate.

Observation windows were constructed of 6.35 mm thick clear lexan in a double pane configuration with a 6.35 mm gap between the panes. The observation windows were constructed so that dry-nitrogen gas could be cycled into the gap between the panes to eliminate condensation. A rubber gasket and a liquid sealant were used to seal the connection between the observation windows and the sides of the test cell.

The temperatures of the heat exchanger and the constant temperature bath were maintained by two recirculating chillers and a coolant flow system. A Lauda Model RC-20 and a Neslab Model CFT-25 were connected to a coolant flow system with plastic tubing insulated with foam pipe insulation. The Lauda chiller had a cooling capacity of 468 W at 0°C with a temperature stability of ± 0.1°C, and the Neslab chiller had a cooling capacity of 340 W at 5°C with a temperature stability of ± 1.0°C. The coolant flow system was designed so that both recirculating chillers could be used to set the initial conditions of the test cell, and then have the Neslab chiller maintain the initial conditions while the Lauda chiller reached the 0°C temperature used for each test. At the start of each experiment, the valves of the coolant flow system were switched so that the coolant from the Lauda chiller flowed to the heat exchanger and coolant from the Neslab chiller flowed to the constant temperature bath. A 1 : 1 mixture of water and ethylene glycol was used as the coolant fluid.

The flow patterns in the enclosure were visualized by a thymol blue pH indicator technique [10]. This technique consists of placing two electrodes in a solution of 0.01% by weight thymol blue and water which has been titrated to the end-point. By imposing a 1.25–3.0 V voltage difference between the electrodes, the fluid next to the positive electrode changes color to a deep blue. The dark blue fluid is then carried away by the fluid flow, and will remain in the flow for a significant length of time, until diffusion effects return the fluid to its original tea color [7]. Density-difference effects are absent in this flow visualization technique, since the thymol blue remains an ion in solution [10]. Therefore the dark fluid exactly follows the flow and measurement of fluid velocities are possible. The test cell was equipped with three pairs of wire electrodes placed horizontally 1.0 cm from the vertical midplane. Each electrode pair consisted of two 0.381 mm diameter copper wires spaced 5 mm apart. The positive electrode of each pair was located at 2.0, 6.0, and 10.0 cm from the bottom of the test cell. A voltage difference was applied to each electrode pair by means of a switch box and a d.c. voltage source. The switch box contained a variable resistor so that the voltage difference between the electrodes could be adjusted to eliminate bubbles at the positive electrode caused by electrolysis. The presence of bubbles caused the dark fluid to rise with the bubbles to the top of the test cell.

The flow visualization experiments were conducted with distilled water which had been mixed with 0.01% by weight thymol blue. Initial conditions were set in the test cell by maintaining the desired initial temperature for 24 h. Once the thermocouple extending into the test cell showed isothermal conditions over time, it was then removed one hour before the start of each experiment. At the start of each experiment the cold water temperature was reduced to 0°C by switching the coolant flow to the heat exchanger from the Neslab to the Lauda chiller, which had been main-

tained at 0°C. At approximately 1 h intervals the insulation was removed from the observation windows and the electrodes were energized, and the transient convective flow patterns were recorded by a video camera for approximately 15 min. This procedure was followed for the first 5 h of each experiment. Steady-state flow patterns were recorded in the same manner after approximately 22 h for each experiment. Experimental velocity measurements were made by reviewing the video tape of the experiment and timing the movement of the dark fluid as it moved away from the electrodes. The distance and angle travelled by the dark fluid was determined by a 1 mm grid that was placed at the opposite observation window. The error in the velocity measurements was ± 0.05 mm s^{-1}. A discussion of the error analysis is given by McDonough [11].

The inlet and outlet temperatures of the heat exchanger and the constant temperature bath were monitored and recorded at 20 min intervals. During each experiment the difference between the inlet and outlet temperatures of the heat exchanger was less than 0.1°C, thus assuring a constant temperature at the cold wall. The difference between the inlet and outlet temperatures of the constant temperature bath varied between ± 0.5°C, which was within the temperature stability of the Neslab chiller.

Two experimental cases were conducted, each with the cold wall maintained at 0°C and the hot wall maintained at 5°C for Case 1 and 8°C for Case 2.

NUMERICAL SIMULATION

The natural convection in a rectangular enclosure of water near its density maximum develops in a complicated manner due to the nonlinear density–temperature relationship. At 3.98°C water has a density maximum, and the coefficient of thermal expansion changes sign. The classical Boussinesq approximation in which the density–temperature relationship of a fluid is assumed to be linear and a factor of the coefficient of thermal expansion, $\rho \simeq \rho_0[1-\beta(T-T_0)]$, is not valid for the natural convection of water near its density maximum. In the present investigation, with a vertical wall height of 120 mm, the natural convection of water in the rectangular enclosure can be classified as high Rayleigh number or boundary layer convection. This type of convection is characterized by vertical thermal boundary layers, which form along the vertical side walls due to a large temperature gradient at the vertical walls, and horizontal thermal layers which form along the adiabatic horizontal walls. At the interior of the enclosure (the core) the fluid is stagnant and thermally stratified [12].

The transient natural convective motion of water in a rectangular enclosure was modelled two-dimensionally. At time $t < 0$, the water is stagnant and at a uniform temperature, T_h, above the density inversion temperature (3.98°C). Both vertical walls are maintained at T_h and the horizontal walls are adiabatic. At time, $t \geqslant 0$, a uniform temperature, $T_c = 0$°C is maintained at the left vertical wall ($x = 0$) and the right vertical wall ($x = L$) is maintained at $T = T_h$. With the assumptions that the flow is two-dimensional, laminar, and incompressible, and the thermophysical properties are independent of temperature, except the density in the buoyancy force, the conservation of mass, momentum, and energy equations for the fluid flow in nondimensional form are:

$$\frac{\partial U}{\partial X} + \frac{\partial V}{\partial Y} = 0 \tag{1}$$

$$\frac{\partial U}{\partial \tau} + \frac{\partial U^2}{\partial X} + \frac{\partial}{\partial Y}(UV) = -\frac{\partial P}{\partial X} + Pr\frac{\partial^2 U}{\partial X^2} + Pr\frac{\partial^2 U}{\partial Y^2} \tag{2}$$

$$\frac{\partial V}{\partial \tau} + \frac{\partial}{\partial X}(UV) + \frac{\partial V^2}{\partial Y} = -\frac{\partial P}{\partial Y} + \frac{H^3 g}{\alpha^2}\left(1-\frac{\rho}{\rho_0}\right) + Pr\frac{\partial^2 V}{\partial X^2} + Pr\frac{\partial^2 V}{\partial Y^2} \tag{3}$$

$$\frac{\partial T^*}{\partial \tau} + U\frac{\partial T^*}{\partial X} + V\frac{\partial T^*}{\partial Y} = \frac{\partial^2 T^*}{\partial X^2} + \frac{\partial^2 T^*}{\partial Y^2}. \tag{4}$$

The nondimensional variables are defined as follows:

$$X = \frac{x}{H} \quad Y = \frac{y}{H} \quad \tau = \frac{\alpha}{H^2}t$$

$$U = u\frac{H}{\alpha} \quad V = v\frac{H}{\alpha}$$

$$T^* = \frac{T-T_c}{T_h-T_c} \quad P = \frac{H^2}{\rho_0\alpha^2}(p+\rho_0 gy).$$

In the nondimensional momentum equations, the Prandtl number appears due to the fact that the driving force for fluid motion is the temperature gradient at the vertical walls of the enclosure, and thus the Prandtl number accounts for the balance between thermal diffusion and momentum diffusion in the fluid.

The nondimensional initial and boundary conditions are

Initial conditions:

$$T^*(X, Y, \tau) = 1 \quad \tau < 0 \tag{5}$$

$$U = V = 0 \quad \tau < 0 \tag{6}$$

Boundary conditions:

$$\text{Cold wall} \quad T^*(0, Y, \tau) = 0 \quad 0 \leqslant Y \leqslant 1, \ \tau \geqslant 0 \tag{7}$$

$$\text{Hot wall} \quad T^*(L/H, Y, \tau) = 1 \quad 0 \leqslant Y \leqslant 1, \ \tau \geqslant 0 \tag{8}$$

$$\text{Adiabatic top} \quad \left.\frac{\partial T^*}{\partial Y}\right|_{Y=1} = 0 \tag{9}$$

$$\text{Adiabatic bottom} \quad \left.\frac{\partial T^*}{\partial Y}\right|_{Y=0} = 0 \tag{10}$$

$$\text{No slip} \quad U = V = 0 \quad Y = 0;\ Y = 1 \tag{11}$$

$$U = V = 0 \quad X = 0;\ X = L/H. \tag{12}$$

The density–temperature relationship for water used in the buoyancy force term of equation (3) was defined by

$$\frac{\rho}{\rho_0} = [1+\beta_1 T+\beta_2 T^2+\beta_3 T^3+\beta_4 T^4]^{-1} \tag{13}$$

where the reference density and coefficients are

$$\rho_0 = 999.8396\,\text{kg m}^{-3}$$

$$\beta_1 = -0.678964520\times 10^{-4}(^\circ\text{C}^{-1})$$

$$\beta_2 = 0.907294338\times 10^{-5}(^\circ\text{C}^{-2})$$

$$\beta_3 = -0.964568125\times 10^{-7}(^\circ\text{C}^{-3})$$

$$\beta_4 = 0.873702983\times 10^{-9}(^\circ\text{C}^{-4}). \tag{14}$$

This density–temperature relationship has been used by previous investigators of the natural convection of water and accurately represents the density as a function of temperature for $0 \leqslant T \leqslant 20^\circ$C [13].

For the natural convection of water, a modified Rayleigh number has been defined as

$$Ra^* = \frac{gH^3}{\alpha\nu}\left|\left(1-\frac{\bar{\rho}}{\rho_0}\right)\right| \tag{15}$$

where $\bar{\rho}$ is the mean density at $(T_h+T_c)/2$. Previous studies have also defined a modified Rayleigh number for the natural convection of water using an inversion parameter in place of the coefficient of thermal expansion [14]. The Rayleigh number is a geometric parameter and the fourth root of the Rayleigh number, $Ra^{1/4}$, is similar to the ratio of the wall height to the thermal boundary layer thickness [12].

The conservation equations were solved numerically using a control-volume based finite-difference formulation [15], where the calculation domain is divided into nonoverlapping control volumes with each control volume surrounding a grid point. The conservation equations (1)–(4), are integrated over each control volume with the assumption that the variation of the dependent variable is linear between grid points. The resulting linear discretization equations were solved at each time step using the line-by-line method and the tridiagonal-matrix algorithm (TDMA) to solve the system of linear equations. Since the momentum and energy equations are coupled through the buoyancy force term, the SIMPLER algorithm [15] was used to iteratively solve the conservation equations. Convergence of the solution for each time step was determined by the relation

$$\left|\frac{\phi^k-\phi^{k+1}}{\phi^k}\right| < 10^{-4} \tag{16}$$

where ϕ is U, V, or T in equations (1)–(4) and k represents the value of the dependent variable at the previous time step and $k+1$ the value at the current time step. The numerical solution was determined to be converged at a time step when all three dependent variables satisfied equation (16).

The grid independence of the numerical solution was analyzed with a uniform grid of 20×20, 30×30, and 40×40. The numerical solution for the temperature was shown to be relatively independent of grid size with a maximum difference between 20×20 and 30×30 cells of 8.9%, and a maximum difference between 30×30 and 40×40 cells of 2.5%. For the v-velocity the maximum difference between 20×20 and 30×30 cells was 27%, whereas the maximum difference between 30×30 and 40×40 cells was 1.4%. For the u-velocity the maximum difference between 20×20 and 30×30 cells was 20% and the maximum difference between 30×30 and 40×40 cells was 11%. A discussion of grid independence is given in McDonough [11].

A number of time steps were tested for $T_h = 5^\circ$C and it was found that with a time step of $\Delta t = 1$ s the solution was relatively independent of time step. With a time step of $\Delta t = 1$ s and a 30×30 grid size, the ratio of simulation time to c.p.u. time was approximately 1/85. For a 40×40 grid size, the ratio of simulation time to c.p.u. time roughly doubled. Thus, due to the large amount of c.p.u. time required to obtain a solution, a 30×30 grid size was used and only the first 5 min of the solutions are presented. The steady-state numerical solutions were obtained by using a false time step method.

The transient and steady-state numerical solutions for the natural convection of water through its density inversion were obtained for a cold wall temperature, $T_c = 0^\circ$C and four initial and hot wall temperatures: Case 1 with $T_i = T_h = 5^\circ$C; Case 2 with $T_i = T_h = 8^\circ$C; Case 3 with $T_i = T_h = 10^\circ$C; and Case 4 with $T_i = T_h = 3.98^\circ$C.

RESULTS AND DISCUSSION

Experimental results are presented for initial and hot wall temperatures of 5 and 8°C. Numerical results are presented for initial and hot wall temperatures of 3.98, 5.0, 8.0, and 10°C. The experimental and numerical results for Case 1 with a 5°C initial and hot wall temperature at $t = 3$ min indicated a strong downward flow near the cold wall by the movement of the dark fluid down from the top of the enclosure. At this early stage of the cooling process, the fluid near the cold wall ($x = 0$) had been cooled to the density inversion, and flows down the cold wall. This sudden downward fluid movement causes fluid to be forced along the bottom of the enclosure and back into the interior due to continuity. Once the fluid near the cold wall has been cooled below the density inversion, the direction of the buoyancy-induced flow was up the cold wall, where the density inversion contour ($T = 3.98^\circ$C) clearly separates the two flow cells. The dark fluid which was generated by the wire

Table 1. Experimental and numerical velocities for Case 1 (T_h = 5°C) at the start of the cooling process

Velocity location		Experimental			Numerical			Test time
x (mm)	y (mm)	$\vec{V}$ (mm s^{-1})	u (mm s^{-1})	v (mm s^{-1})	$\vec{V}$ (mm s^{-1})	u (mm s^{-1})	v (mm s^{-1})	(min)
106	68	0.13	−0.07	0.11	0.10	−0.05	0.09	3
118	28	0.14	−0.07	0.12	0.13	0.07	0.11	3
115	10	0.42	0.42	0.0	0.50	0.49	0.02	2

electrodes was swept into the faster moving fluid at the density inversion. The bulk fluid motion down the cold wall and back into the interior was also indicated by the numerical temperature contours, in which the colder fluid was driven down and along the bottom of the enclosure.

At t = 5 min, the dominant flow pattern was still the large counterclockwise rotating flow cell which extends from the density inversion to the hot wall, as shown in Fig. 2(a). The smaller clockwise rotating flow cell below the density inversion was evidenced by the dark line of fluid at the bottom left corner of Fig. 2(a). The experimental flow patterns, numerical velocity vectors and temperature contours all show the movement of the colder fluid downward and across the bottom of the enclosure, where the fluid at the interior was forced upward. The experimental and numerical velocities of this bulk fluid motion back into the interior of the enclosure are given in Table 1, and are in good agreement. In Table 1, the resultant velocities, $\vec{V}$, are given along with the component velocities. At x = 118 and y = 28, the experimental and numerical u-velocity component showed a difference in direction, which was due to the assumption in the numerical solution of an instantaneous temperature change at the cold wall. The numerical results show that during this early stage the maximum velocities occur at the density inversion as shown in Fig. 2(b). This is also indicated in the experimental flow patterns (Fig. 2(a)) by the dark line of fluid near the cold wall. For Case 1 with a 5°C initial and hot wall temperature, the numerical and experimental flow patterns shown in Fig. 2 are in good agreement. Due to the large amount of computer time required, only the first 5 min of the numerical solution are presented.

After the initial stage of cooling, the clockwise rotating flow cell below the density inversion expands across the enclosure. Figure 3 shows the experimental flow pattern at t = 90 min. Two flow cells are clearly indicated in Fig. 3(a) where the clockwise rotating flow cell was below the density inversion and the counterclockwise rotating flow cell was above the density inversion. The flow cells are shown schematically in Fig. 3(b) along with the experimental velocity measurements. As can be seen in Fig. 3(a), the maximum fluid velocities occur along the vertical walls where the dark fluid was swept away quickly. At the interior of the flow cells, the fluid was relatively stagnant which was indicated by the dark fluid remaining at the electrodes. Due to the limitations of the thymol blue pH indicating technique, specifically the fact that the dark fluid dispersed quickly in the regions of the maximum fluid velocities and thus making velocity measurements difficult, the experimental velocity measurements reported are at the boundaries of the faster moving fluid at the walls.

As the cooling process continued, the clockwise rotating flow cell expanded across the enclosure until at t = 150 min, it encompassed the majority of the enclosure, as shown in Fig. 4. A small counterclockwise rotating flow cell was evident in Fig. 4(a) by the dispersion of the dark fluid at the center electrode pair at the right vertical wall. The schematic of this flow pattern is shown in Fig. 4(b) along with the experimental velocity measurements. Again the maximum velocity occurred at the vertical walls where the dark fluid was swept away quickly and the interior of the enclosure contains relatively stagnant fluid.

The steady-state experimental and numerical results are shown in Fig. 5 for Case 1, T_h = 5°C. Figure 5(a) shows the experimental flow pattern after 22 h of cooling, in which a clockwise rotating flow cell encompasses the entire enclosure except at the bottom of the hot wall where a small counterclockwise rotating flow cell exists. The steady-state numerical results in Fig. 5(b) predict the same type of flow pattern and are in good agreement with the experimental flow pattern in Fig. 5(a). Numerical temperature contours in Fig. 5(c) show the distinct thermal boundary layers at the vertical walls and a thermally stratified interior core region, in which the colder and lighter fluid was above the hotter and heavier fluid, indicating the interior was in a stable condition. Experimental velocity measurements are in good agreement with numerical results for steady-state conditions as shown in Table 2.

In Case 1, the influence of the density inversion had a significant effect on the transient convective fluid motion during the early periods of cooling. This was evidenced by the expansion of a clockwise rotating flow cell from the cold wall (Fig. 2) and across the enclosure (Fig. 3) until at steady state when this flow cell encompasses the majority of the enclosure (Fig. 5).

The experimental and numerical results for Case 2 with an 8°C initial and hot wall temperature at t = 3 min showed that the cooling process was characterized by a strong downward fluid movement at the cold

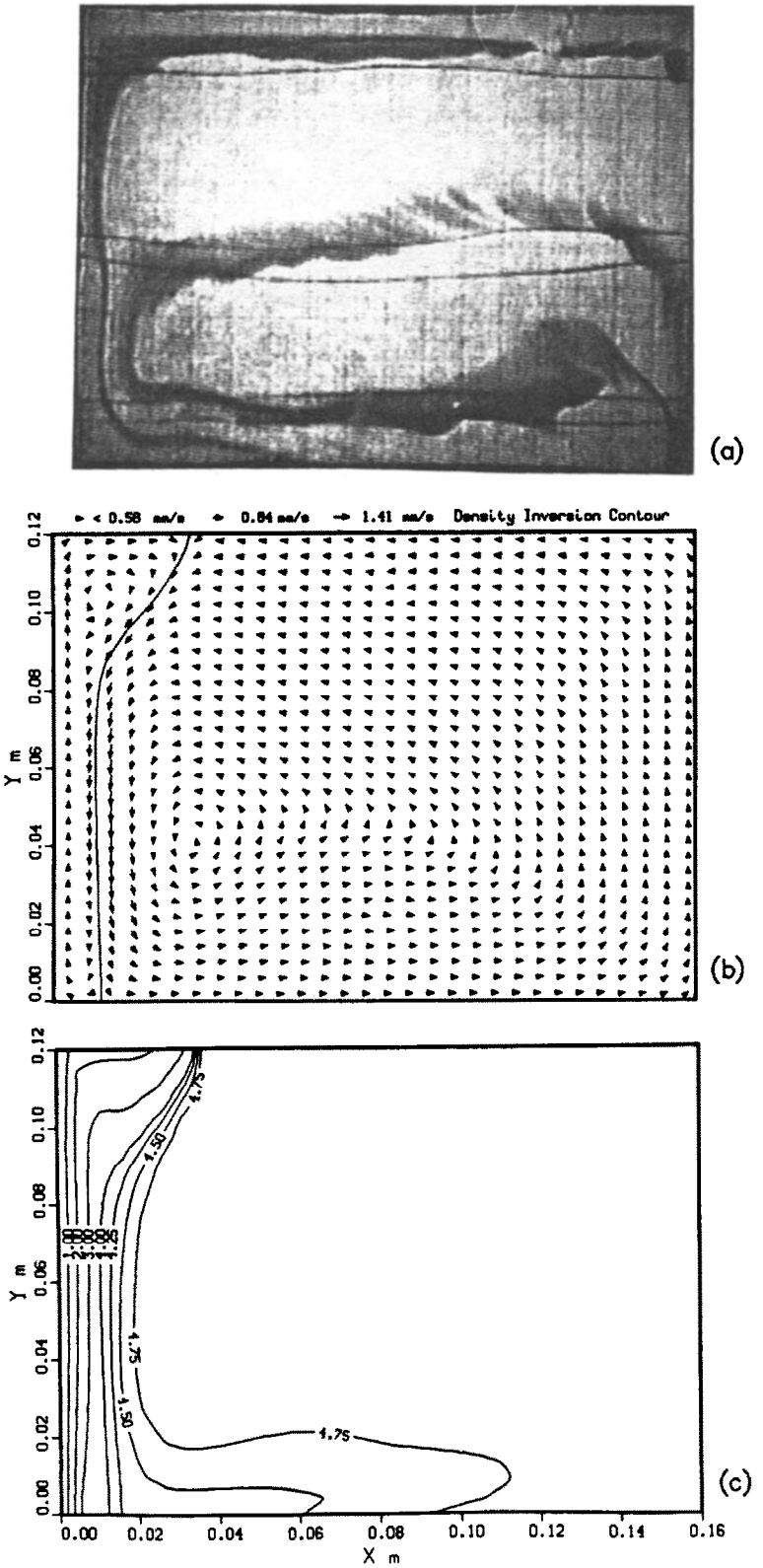

FIG. 2. Transient flow patterns and temperature contours, Case 1 ($T_h = 5°C$) at $t = 5$ min : (a) experimental flow pattern ; (b) numerical velocity vectors ; and (c) numerical temperature contours.

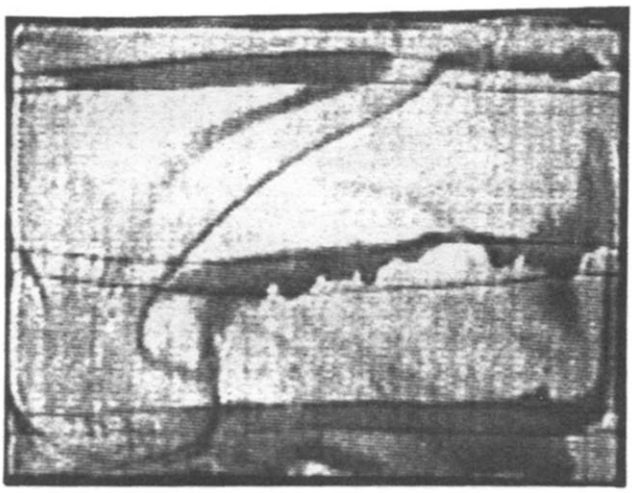

(a)

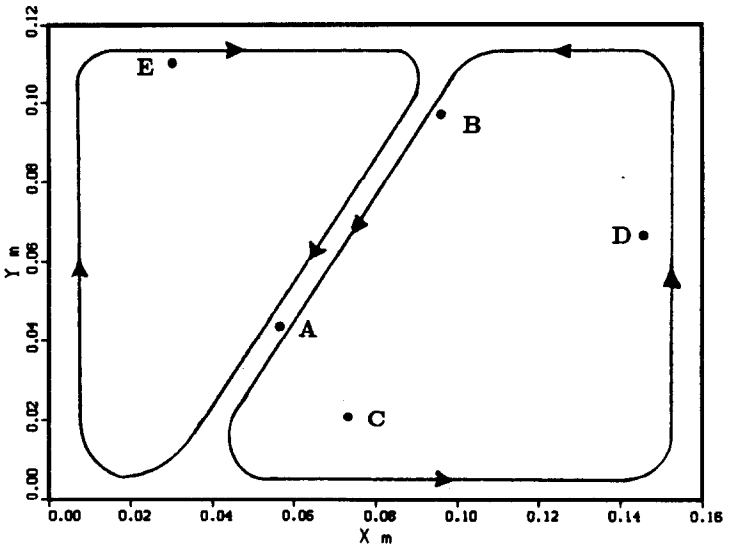

(b)

Location			$\vec{V}$	u	v
	x (mm)	y (mm)	(mm/s)	(mm/s)	(mm/s)
A	43	44	0.22	-0.17	-0.14
B	90	103	0.55	-0.49	-0.26
C	72	21	0.22	0.22	0.0
D	150	75	0.13	0.0	0.13
E	25	115	0.25	0.24	0.06

FIG. 3. Experimental transient flow patterns, Case 1 ($T_h = 5^\circ C$) at $t = 90$ min: (a) experimental flow pattern; (b) schematic of flow pattern and velocity measurement locations.

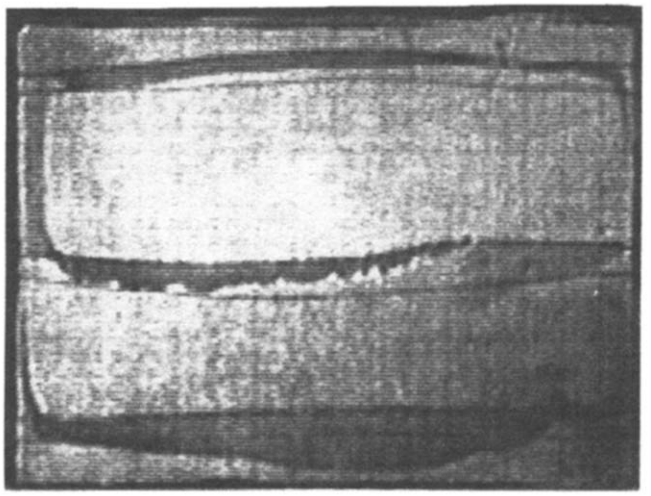

(a)

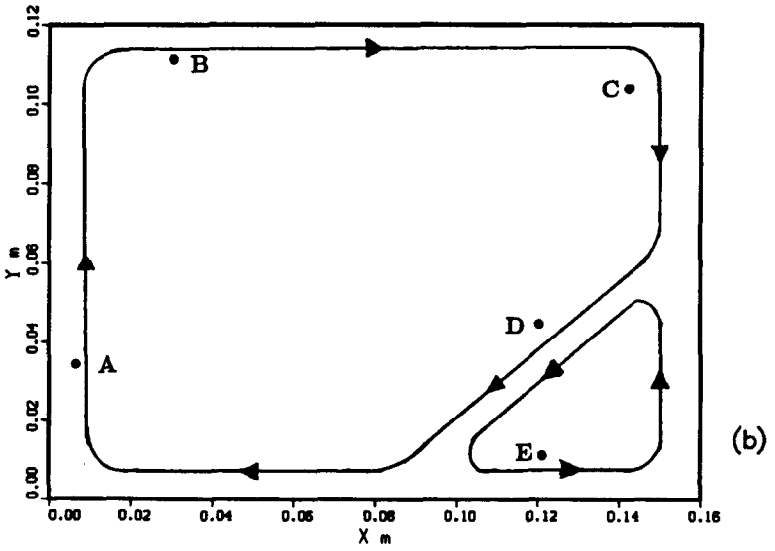

(b)

Location			$\vec{V}$	u	v
	x (mm)	y (mm)	(mm/s)	(mm/s)	(mm/s)
A	6	35	0.24	0.0	0.24
B	31	116	0.27	0.27	0.0
C	145	102	0.17	0.05	-0.16
D	126	45	0.42	-0.25	-0.34
E	122	12	0.10	0.04	-0.09

FIG. 4. Experimental transient flow patterns, Case 1 ($T_h = 5°C$) at $t = 150$ min: (a) experimental flow pattern; (b) schematic of flow pattern and velocity measurement locations.

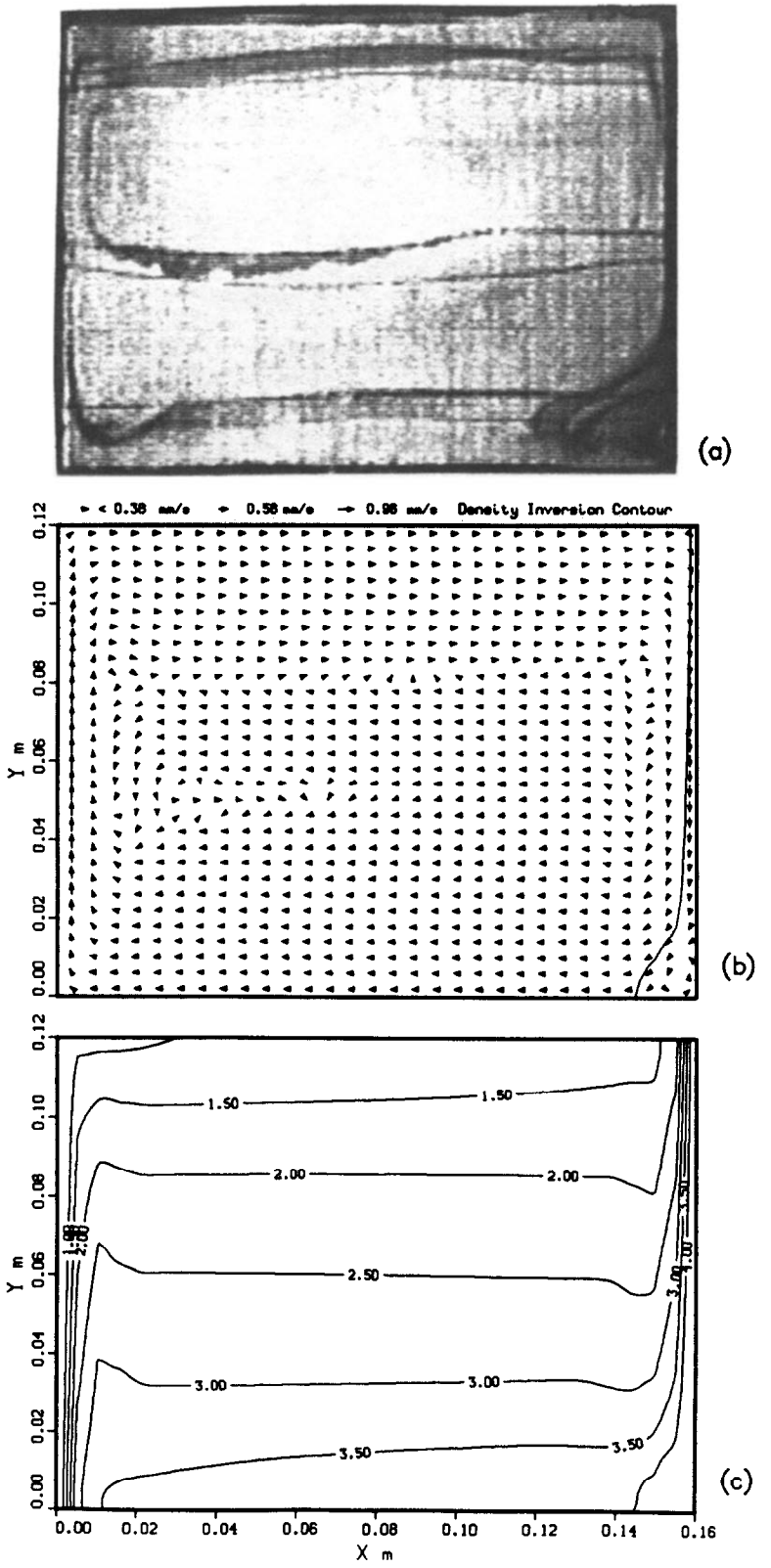

FIG. 5. Steady-state flow patterns and temperature contours Case 1 ($T_h = 5°C$): (a) experimental flow pattern; (b) numerical velocity vectors; and (c) numerical temperature contours.

Table 2. Steady-state experimental and numerical velocities for Case 1 ($T_h = 5°C$)

Velocity location		Experimental			Numerical		
x (mm)	y (mm)	$\bar{V}$ (mm s^{-1})	u (mm s^{-1})	v (mm s^{-1})	$\bar{V}$ (mm s^{-1})	u (mm s^{-1})	v (mm s^{-1})
152	101	0.18	0.04	−0.17	0.18	0.12	−0.14
9	30	0.29	−0.05	0.28	0.30	−0.07	0.29
28	110	0.23	0.23	0.0	0.25	0.25	0.0
151	57	0.20	0.0	−0.20	0.23	0.0	−0.23

wall which then flowed along the bottom and was dispersed into the interior. Figure 6 shows the experimental flow pattern and the numerical results at $t = 5$ min, which are in good agreement. The experimental flow pattern in Fig. 6(a) shows the continuation of the downward fluid movement at the cold wall and back into the interior of the enclosure. In Fig. 6(b), the numerical results show a similar flow pattern. Numerical temperature contours in Fig. 6(c) also indicate the movement of the cooled fluid into the interior. A comparison of the experimental and numerical velocities for the fluid motion back into the interior is given in Table 3. This bulk fluid motion from the cold wall and into the interior of the enclosure at the beginning of the cooling process has also been reported by Braga and Viskanta [8] for the natural convection of water near its density maximum in a rectangular cavity.

After the initial period of cooling, the influence of the density inversion on the convective flow increases until a clockwise rotating flow cell forms at the cold wall. Figure 7(a) shows the experimental flow pattern at $t = 90$ min where the flow pattern was characterized by two counter rotating flow cells. At the cold wall, a clockwise rotating flow cell exists with the fluid in the cell below the density inversion, and a counterclockwise rotating flow cell with the fluid above the density inversion exists at the hot wall. These two flow cells are shown schematically in Fig. 7(b) with the experimental velocity measurements.

At $t = 150$ min, experimental flow patterns indicated that the influence of the density inversion had diminished with the clockwise rotating flow cell at the cold wall decreasing in size. This change in the convective flow pattern was due to the fact that during the early period of the cooling process the temperature gradient at the cold wall was the dominant driving force for the buoyancy-induced flow. After this early period, a steep temperature gradient forms at the hot wall and drives the convective flow above the density inversion.

The experimental flow patterns at $t = 300$ min showed that the convective fluid motion in the enclosure was approaching a steady condition. The steady-state experimental flow pattern and numerical results are shown in Fig. 8. After 22 h of cooling, the copper heat exchanger at the cold wall was used as the positive electrode for flow visualization. Figure 8(a) shows the clockwise rotating flow cell at the cold wall. By using the copper heat exchanger as the positive electrode, the dark fluid generated at the cold wall remained in the flow cell and thus marked the flow which was below the density inversion. The steady-state numerical results in Fig. 8(b) show a similar flow cell at the cold wall with a large counterclockwise rotating flow cell in the majority of the enclosure. In Fig. 8(c), the numerical temperature contours show steep temperature gradients at the vertical walls with a thermally stratified interior, which are also indicated by the experimental flow patterns in Fig. 8(a) by the strong upward fluid flow at the hot wall driven by the temperature gradient and the relative stagnant fluid in the interior due to the thermal stratification. The comparison between the experimental and numerical velocities is given in Table 4. The difference between the numerical and experimental velocities, at $x = 26$ mm and $y = 56$ mm, and $x = 25$ mm and $y = 17$ mm where the two flow cells meet, was due to the fact that the numerical solution used a relatively coarse grid. With a coarse grid and the rapid change in temperature and velocity occurring in this region, the numerical solution was unable to capture the finer details of the

Table 3. Experimental and numerical velocities for Case 2 ($T_h = 8°C$) at the start of the cooling process

Velocity location		Experimental			Numerical			Test time (min)
x (mm)	y (mm)	$\bar{V}$ (mm s^{-1})	u (mm s^{-1})	v (mm s^{-1})	$\bar{V}$ (mm s^{-1})	u (mm s^{-1})	v (mm s^{-1})	
119	35	0.36	−0.22	0.29	0.38	0.10	0.37	3
109	65	0.29	−0.23	0.17	0.35	−0.19	0.30	3

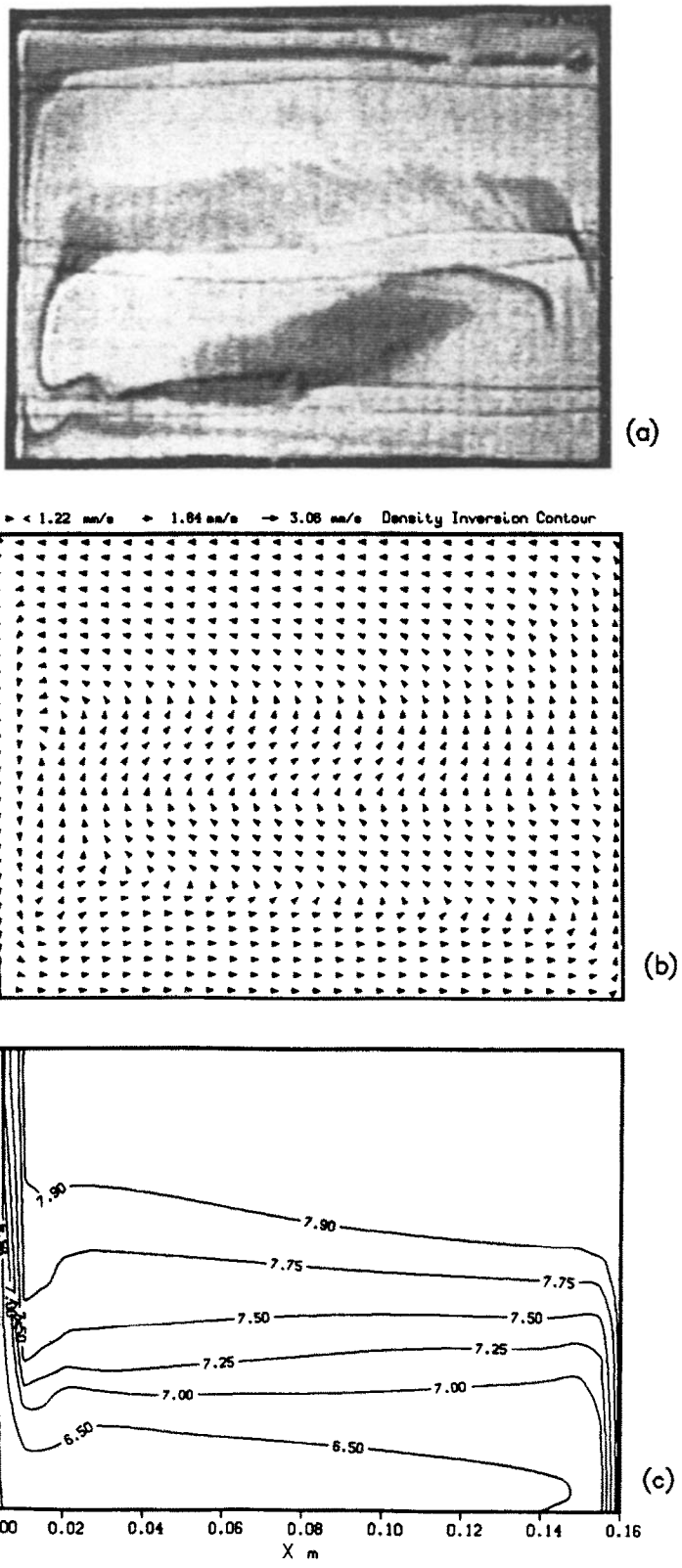

FIG. 6. Transient flow patterns and temperature contours, Case 2 ($T_h = 8°C$) at $t = 5$ min : (a) experimental flow pattern ; (b) numerical velocity vectors ; and (c) numerical temperature contours.

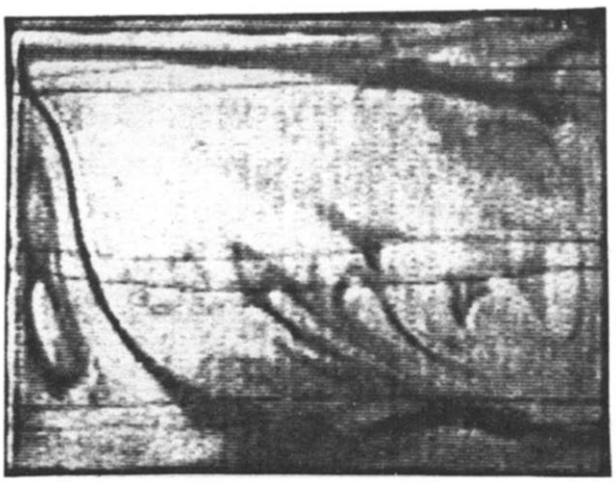

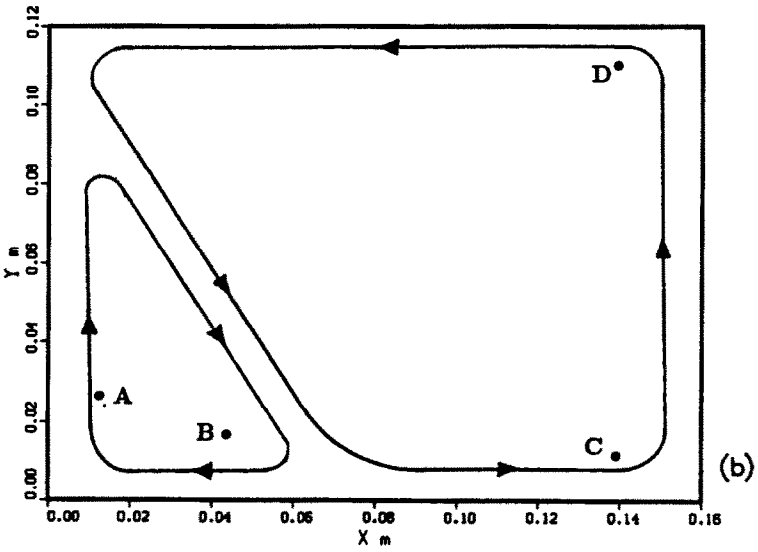

Location			$\vec{V}$	u	v
	x (mm)	y (mm)	(mm/s)	(mm/s)	(mm/s)
A	8	27	0.27	0.0	0.27
B	41	17	0.22	0.03	-0.22
C	143	11	0.24	0.21	-0.12
D	144	111	0.12	-0.11	0.05

FIG. 7. Experimental transient flow patterns, Case 2 ($T_h = 8°C$) at $t = 90$ min: (a) experimental flow pattern; (b) schematic of flow pattern and velocity measurement locations.

Table 4. Steady-state experimental and numerical velocities for Case 2 ($T_h = 8°C$)

Velocity location		Experimental			Numerical		
x (mm)	y (mm)	$\vec{V}$ (mm s^{-1})	u (mm s^{-1})	v (mm s^{-1})	$\vec{V}$ (mm s^{-1})	u (mm s^{-1})	v (mm s^{-1})
26	56	0.21	0.0	−0.21	0.44	0.07	−0.43
25	17	0.23	0.0	−0.23	0.38	0.27	−0.27
149	66	0.24	0.0	0.24	0.30	0.04	0.29

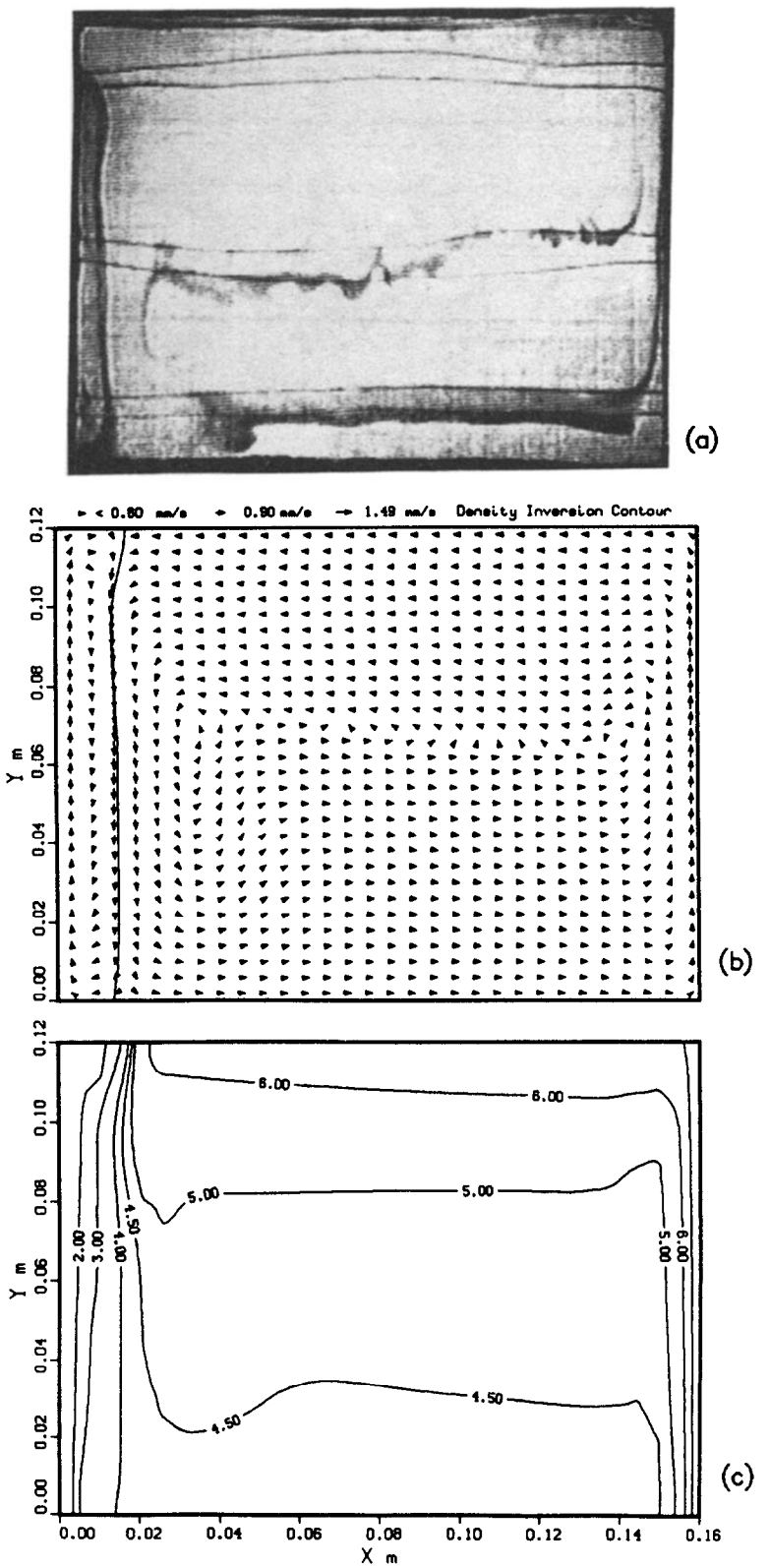

FIG. 8. Steady-state flow patterns and temperature contours, Case 2 ($T_h = 8°C$): (a) experimental flow pattern; (b) numerical velocity vectors; and (c) numerical temperature contours.

convective flow. Away from this region, there was good agreement between the experimental and numerical results.

Previous studies of the natural convection of water near its density inversion in a rectangular enclosure have also shown that the steady-state flow patterns with a hot wall temperature of 8°C were characterized by two counter rotating flow cells. At an 8°C hot wall temperature, a symmetrical flow pattern about the vertical centerline has been shown to exist at steady-state for a square enclosure numerically by Watson [2] and experimentally by Inaba and Fukuda [6]. The results of the present study indicate that this symmetrical flow pattern does not occur for the rectangular enclosure. The reason for asymmetrical flow pattern is related to the effect of the boundary layers at the vertical walls on the fluid at the interior of the enclosure and the size of the enclosure. With the large Rayleigh number (1.25×10^7) in the present study, the thicknesses of the boundary layers at the vertical walls were small compared to the size of the enclosure, and the influence of the boundary layers was minimal on the interior fluid. In the studies by Watson [2], and Inaba and Fukuda [6], the Rayleigh numbers were of the order of 2×10^4. With a small Rayleigh number the thicknesses of the boundary layers were large compared to the size of the enclosure and the boundary layers had a dominant influence on the interior fluid. In the experimental study by Inaba and Fukuda [6] the dimension of the square enclosure was

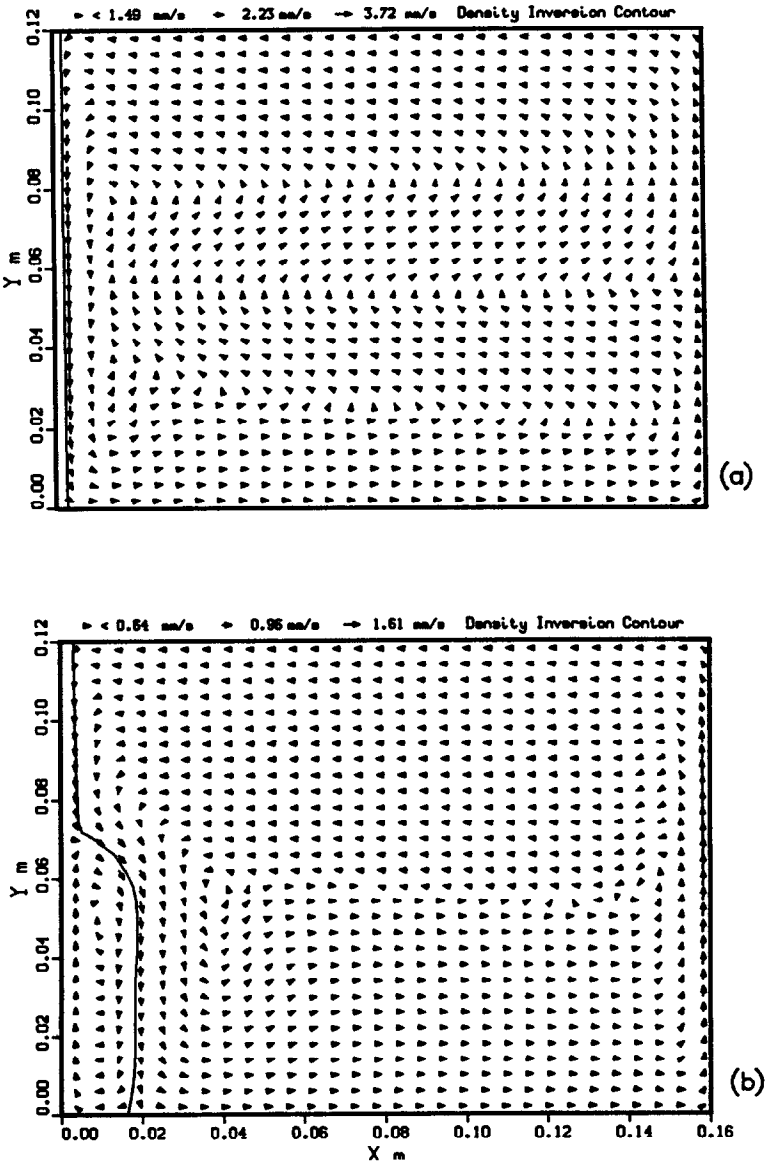

FIG. 9. Numerical velocity vectors, Case 3 ($T_h = 10°C$): (a) $t = 5$ min; and (b) steady-state.

15 mm whereas in the present study the dimension was 120×160 mm ($H \times L$) with an aspect ratio of 0.75. This asymmetrical flow pattern was also seen by Braga and Viskanta [8] during the transient cooling of water in an open rectangular cavity with an aspect ratio of 0.5, a dimension of 150×300 mm ($H \times L$), and $Ra = 6.6 \times 10^7$.

The numerical results for Case 3 with a 10°C initial and hot wall temperature are presented in Figs. 9 and 10. At the early stage ($t \leqslant 5$ min) of the cooling process, the convection in the enclosure was characterized by the downward fluid flow at the cold wall as the fluid was cooled to the density inversion (Fig. 9(a)). With a 10°C initial temperature, this early stage was dominated by conduction at the cold wall as shown by the parallel temperature contours at the cold wall in Fig. 10(a). At steady-state the numerical results for Case 3 show that the flow cell above the density inversion dominated the convection in the enclosure and the effect of the density inversion was shown by the existence of the clockwise flow cell at the bottom of the cold wall as shown in Fig. 9(b). The steady-state temperature contours in Fig. 10(b) show that the section of the enclosure dominated by the flow cell above the density inversion had thermal boundary layers at the vertical sides and was thermally stratified in the interior.

The numerical results for Case 4 with an initial and hot wall temperature at the density inversion, 3.98°C, are presented in Figs. 11 and 12. This case illustrates

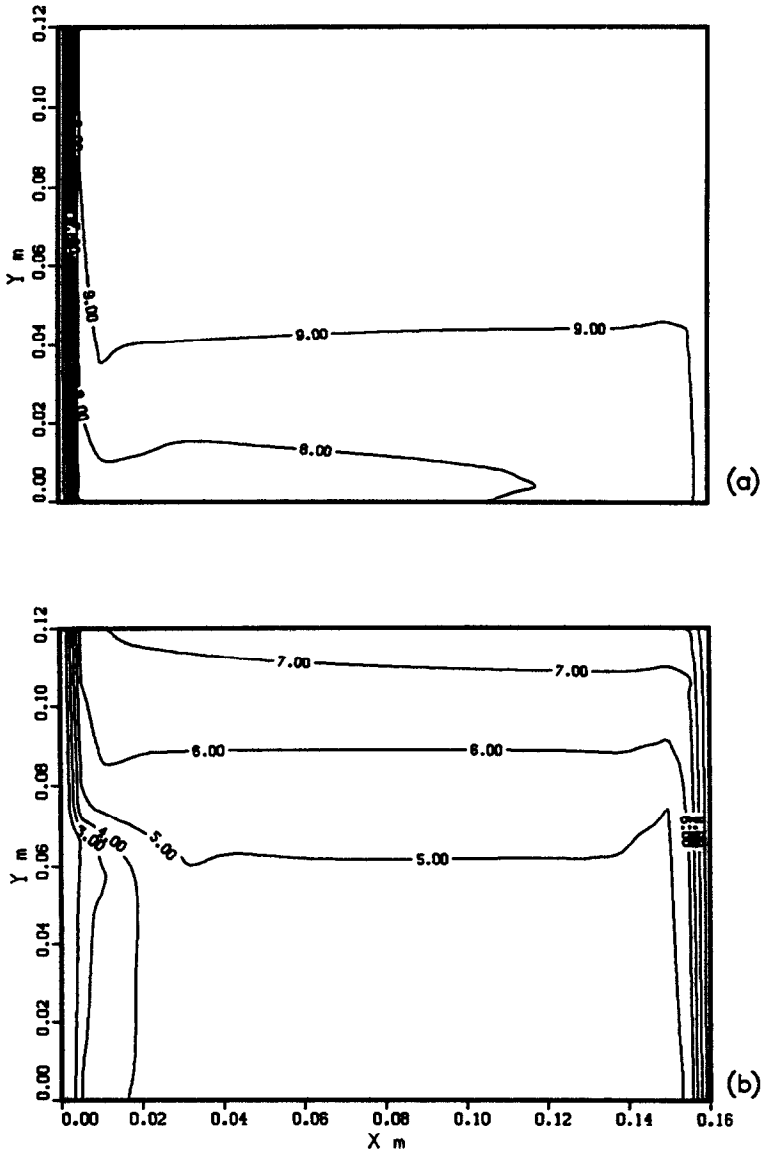

FIG. 10. Numerical temperature contours, Case 3 ($T_h = 10$°C): (a) $t = 5$ min; and (b) steady-state.

the natural convection of water in the enclosure without the density inversion. As the fluid in the enclosure was cooled, the fluid near the cold wall was driven up and along the top, with the maximum velocities occurring at the cold wall as shown in Fig. 11(a) at $t = 5$ min. This is also seen in Fig. 12(a) where the temperature contours show the colder fluid expanding along the top of the enclosure. At steady-state the flow pattern in the test cell was symmetrical with a clockwise flow cell encompassing the entire enclosure (Fig. 11(b)). The temperature contours at steady-state also indicated this symmetry by the 2°C contour line being at the center of the enclosure and the similar contours of the temperature gradients at each vertical wall as shown in Fig. 12(b).

CONCLUSIONS

The transient and steady state natural convection of water near the density inversion in a rectangular enclosure has been investigated experimentally and numerically. Numerical results were presented for initial and hot wall temperatures of 3.98, 5.0, 8.0, and 10.0°C. Experimental flow patterns were obtained for initial and hot wall temperatures of 5 and 8°C. The results of the investigation can be summarized as follows.

1. The influence of the density inversion was dominant during the transient period with $T_i = T_h = 5$°C due to the expansion of a clockwise flow cell below the density inversion across the enclosure.

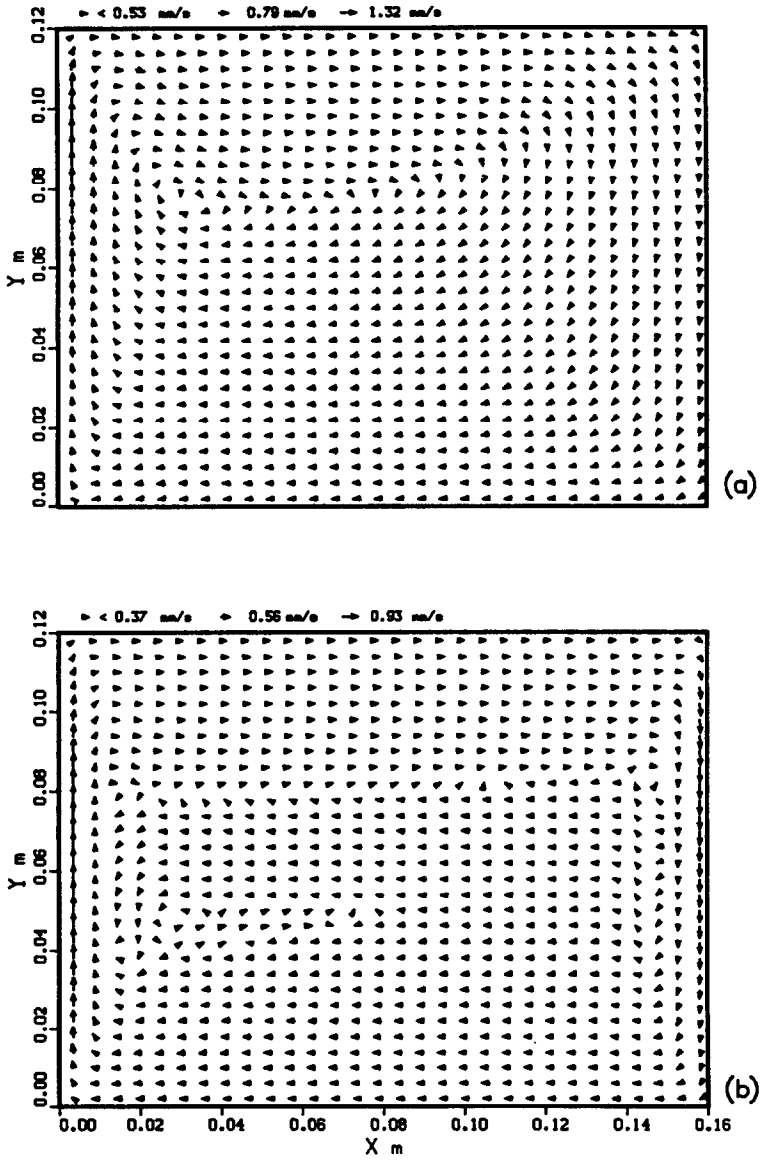

FIG. 11. Numerical velocity vectors, Case 4 ($T_h = 3.98$°C): (a) $t = 5$ min; and (b) steady-state.

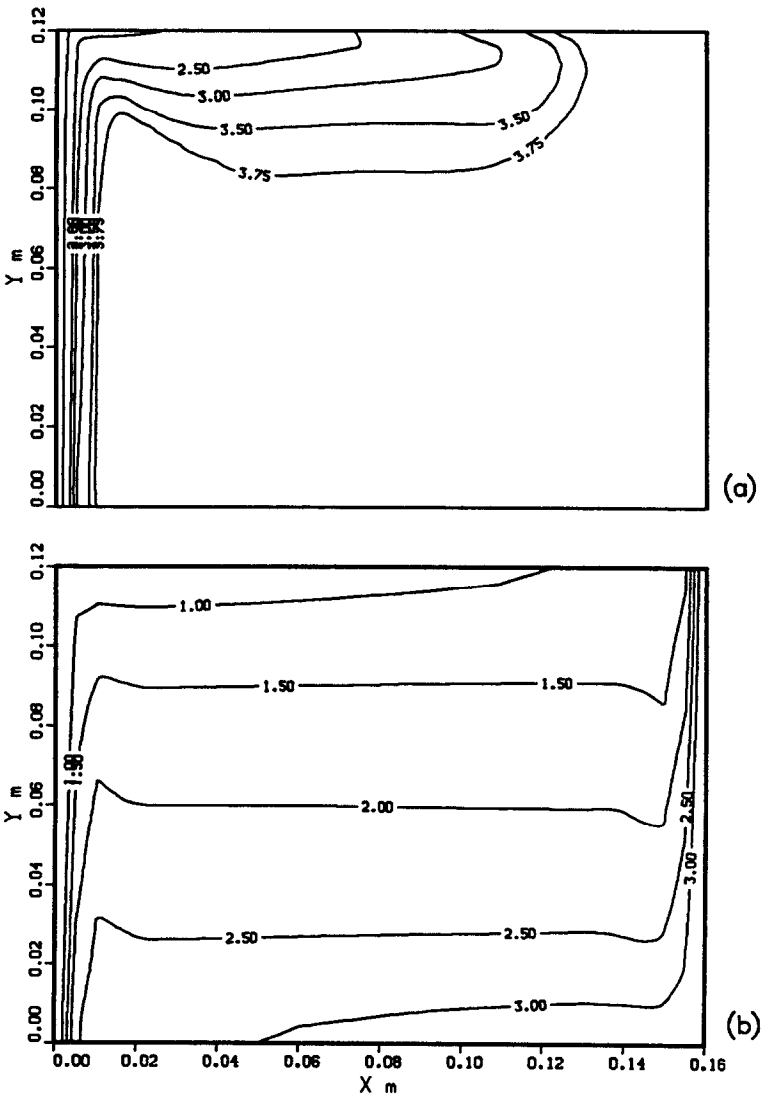

FIG. 12. Numerical temperature contours, Case 4 ($T_h = 3.98°C$): (a) $t = 5$ min; and (b) steady-state.

2. The effect of the density inversion on the convective flow patterns in the enclosure was to produce two counter rotating cells in Case 1 with a 5°C initial and hot wall temperature, and in Case 2 with an 8°C initial and hot wall temperature.

3. The asymmetric convective flow patterns in the enclosure at $T_i = T_h = 8°C$ indicate that the symmetrical flow patterns predicted by previous investigators does not develop due to the large *Ra* and the small influence of the boundary layers at the vertical walls on the interior fluid.

REFERENCES

1. S. Ostrach, Natural convection in enclosures, *ASME J. Heat Transfer* **110,** 1175 (1988).
2. A. Watson, The effect of the inversion temperature on the convection of water in an enclosed rectangular cavity, *Q. J. Mech. Appl. Math.* **25**(4), 423 (1972).
3. K. C. Cheng and M. Takeuchi, Transient natural convection of water in a horizontal pipe with constant cooling rate through 4°C, *ASME J. Heat Transfer* **98,** 581 (1976).
4. P. Vasseur and L. Robillard, Transient natural convection heat transfer in a mass of water cooled through 4°C, *Int. J. Heat Mass Transfer* **23,** 1195 (1980).
5. P. Vasseur, L. Robillard and P. Chandra Shekar, Natural convection heat transfer within a horizontal cylindrical annulus with density inversion effects, *ASME J. Heat Transfer* **105,** 117 (1983).
6. H. Inaba and T. Fukuda, An experimental study of natural convection in an inclined rectangular cavity filled with water at its density extremum, *ASME J. Heat Transfer* **106,** 109 (1984).
7. K. E. Lankford and A. Bejan, Natural convection in a vertical enclosure filled with water near 4°C, *ASME J. Heat Transfer* **108,** 755 (1986).

8. S. L. Braga and R. Viskanta, Transient natural convection of water near its density extremum in a rectangular cavity, *Int. J. Heat Mass Transfer* **35,** 861 (1992).
9. M. McDonough and A. Faghri, Ultrasonic measurement of solid–liquid interface for the solidification of water in a rectangular enclosure, *Proc. of 1993 National Heat Transfer Conference*, Paper No. 93-HT-31, Atlanta, GA (1993). Also *ASME J. Heat Transfer* **115**(4), 1075–1078 (1993).
10. D. J. Baker, A technique for precise measurement of small fluid velocities, *J. Fluid Mech.* **26**(3), 573 (1966).
11. M. McDonough, Solidification and natural convection in enclosures, M.S. Thesis, Wright State University, Dayton, Ohio (1992).
12. A. Bejan, *Convection Heat Transfer*. Wiley, New York (1984).
13. T. Fujii, Fundamentals of free convection heat transfer, *Prog. Heat Transfer Engng* **3,** 66 (1974).
14. K. C. Cheng, H. Inaba and R. R. Gilpin, Effects of natural convection on ice formation around an isothermally cooled horizontal cylinder, *ASME J. Heat Transfer* **110,** 931 (1988).
15. S. V. Patankar, *Numerical Heat Transfer and Fluid Flow*. Hemisphere, New York (1980).